Composite Design and Friction-Wear Characteristics of High-Efficiency Transmission Gear Materials

Zhongyuan Li[1], Xiaoyan Mi[1*]
[1]School of Automotive Engineering, Shanghai Communications Polytechnic No. 763, Hulan Road Baoshan District, Shanghai 200431, China
Corresponding author: Xiaoyan Mi (e-mail: michenhello@163.com)

ABSTRACT To meet the high-speed and heavy-load service requirements of high-efficiency transmission gears, Fe-2Ni iron-based powder metallurgy was used as the matrix, and a composite system reinforced by TiC hard phase and MoS_2 solid lubricant was designed. The gear composites were prepared by hot pressing sintering. The effects of reinforcement ratio and sintering parameters on microstructure and mechanical properties were studied, and the friction and wear behaviors under different loads, sliding speeds and lubrication conditions were investigated. The results show that the optimal sintering process is 1150 °C, 60 min and 30 MPa, with a relative density of 98.6% and microhardness of HV 620. The composite with 10 wt% TiC and 3 wt% MoS_2 exhibits the best comprehensive performance, with a friction coefficient as low as 0.08 and a wear rate reduced by 62% compared with the matrix. The wear mechanism transforms from abrasive wear to oxidative wear and slight delamination wear. The composite presents excellent friction reduction and wear resistance, which can provide a quantitative reference for the design of high-performance transmission gears.

INDEX TERMS Transmission gear; Iron-based composite; Friction and wear; Powder metallurgy; Hot pressing sintering

I. INTRODUCTION

As a key load-bearing component in the power transmission system, transmission gears operate for a long time under complex conditions including high contact stress, high sliding speed and periodic impact load. Its friction and wear performance directly determines the transmission efficiency and service life. Traditional carburized and quenched steel gears have high surface hardness, but still face problems such as high friction coefficient and insufficient wear resistance under extreme working conditions. Introducing hard reinforcement and solid lubricant to construct metal matrix composites is an effective way to break through the performance limitations of existing gear materials. Iron-based powder metallurgy composites have the advantages of strong compositional designability and good near-net-shape forming effect, showing prominent application potential in gear materials. At present, there is still a lack of quantitative influence of reinforcement ratio on friction and wear properties, as well as systematic research on the evolution of wear mechanism under different working conditions. Therefore, the preparation, characterization and friction-wear characteristics of TiC/MoS_2 composite reinforced iron-based gear materials are of important theoretical value and engineering significance.

A. CONSTRUCTION AND COMPOSITION DESIGN OF GEAR COMPOSITE SYSTEM

Iron-based powder metallurgy materials are the preferred matrix for transmission gear composites due to their adjustable composition and high near-net-shape efficiency. Three typical iron-based alloy powders, Fe, Fe-2Ni and Fe-4Ni, were selected for basic performance comparison [1]. The bending strength, hardness and impact toughness were measured by universal testing machine, microhardness tester and impact tester. The results show that Fe-2Ni matrix achieves the best balance between hardness and toughness: Vickers hardness HV 312, bending strength 820 MPa, impact energy 28 J, and its comprehensive performance is significantly better than pure iron matrix. Although Fe-4Ni has slightly higher hardness (HV 345), its impact toughness decreases obviously, leading to the risk of brittle fracture under periodic impact conditions of transmission gears, so it is not adopted [2]. Fe-2Ni is selected as the matrix of the subsequent composite system, which not only ensures the mechanical strength of the bearing framework, but also provides sufficient plastic basis for the stable distribution of the reinforcement phase, See Table 1.

TABLE 1. Mechanical Properties of Different Iron-Based Matrix Materials

Matrix	HV	Bending strength/MPa	Impact energy/J	Relative density/%
Fe	265	680	35	97.1
Fe-2Ni	312	820	28	98.0
Fe-4Ni	345	875	18	98.3

B. RATIO OPTIMIZATION OF TIC REINFORCEMENT AND MOS_2 LUBRICANT

After determining the Fe-2Ni matrix, TiC (particle size $\sim$2 μm) and MoS_2 ($\sim$5 μm) were introduced into the composite system as hard reinforcement and solid lubricant respectively. TiC is introduced to improve the hardness and wear resistance of the matrix, while the low shear strength of MoS_2 layered crystal structure enables it to form a lubricating transfer film on the friction interface, thus reducing the friction coefficient. The mass fraction of TiC was designed as 5%, 10% and 15%, and MoS_2 was fixed at 3 wt%. The comprehensive friction reduction and wear resistance of each combination were evaluated by orthogonal experiment. When TiC content increases from 5% to 10%, the wear rate decreases from 4.8×10^{-5} mm^3/(N·m) to 1.8×10^{-5} mm^3/(N·m). When TiC further increases to 15%, obvious agglomeration occurs, the interfacial bonding strength decreases, and the wear rate rises to 2.6×10^{-5} mm^3/(N·m). Therefore, the optimal TiC content is 10 wt% [3]. The theoretical density of the composite system is calculated according to the mixture rule:

$$\rho_c = \sum_{i=1}^{n} V_i \cdot \rho_i, \quad (1)$$

where ρ_c is the theoretical density (g/cm^3), V_i and ρ_i are the volume fraction and density of the i component, respectively.

C. INTERFACIAL BONDING MECHANISM AND DESIGN PRINCIPLE

The interfacial bonding quality between TiC reinforcement and Fe-2Ni matrix directly determines the comprehensive mechanical properties of composites. SEM and EDS analysis show that TiC particles form a metallurgical bonding interface with the matrix after hot pressing sintering, without obvious pores or cracks [4]. Ti and Fe interdiffuse at the interface with a diffusion layer thickness of about 0.3–0.5 μm, which effectively enhances the interfacial bonding strength. MoS_2 has relatively low thermal stability and will partially decompose into MoO_3 during sintering. To control its decomposition, the sintering temperature must be strictly controlled below 1150 °C. The stress transfer efficiency of the reinforcement phase under load is estimated by the modified Shear-Lag model:

$$\sigma_c = \sigma_m(1 - V_f) + \sigma_r \cdot V_f \cdot \eta, \quad (2)$$

where σ_c is the bearing stress of the composite, σ_m and σ_r are the stresses of the matrix and reinforcement phase respectively, and η is the interfacial load transfer efficiency factor, See Figure 1.

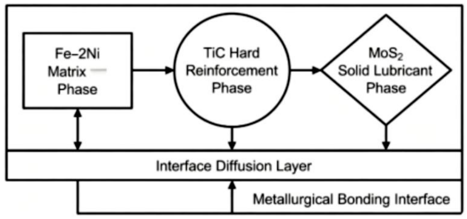

FIGURE 1. Schematic diagram of composition and interfacial bonding structure of TiC/MoS_2/Fe-2Ni composite

TABLE 2. Variable Definition

Temperature/°C	Time/min	Pressure/MPa	Relative density/%	Micro-hardness/HV
1050	60	30	93.8	542
1100	60	30	96.4	578
1150	60	30	98.6	620
1200	60	30	97.9	598
1150	30	30	97.1	601
1150	90	30	98.4	615

II. PREPARATION, MICROSTRUCTURE AND PROPERTIES OF COMPOSITES

A. HOT PRESSING SINTERING PROCESS

Hot pressing sintering (HPS) promotes diffusion and densification between powder particles through the synergy of temperature and pressure [5]. Orthogonal experiments were carried out with sintering temperature (1050–1200 °C), holding time (30–90 min) and sintering pressure (20–40 MPa) as variables, and relative density and microhardness as response indexes. The results show that when the sintering temperature is 1150 °C, holding time 60 min and pressure 30 MPa, the relative density reaches 98.6% and microhardness HV 620. When the temperature exceeds 1180 °C, MoS_2 decomposes seriously [6], reducing the effective lubricant content. The heating rate is controlled at 10 °C/min, and high-purity Ar gas is introduced to prevent oxidation. See Table 2.

B. QUANTITATIVE CHARACTERIZATION OF THE DENSITY, HARDNESS, AND MICROSTRUCTURE OF COMPOSITE MATERIALS

The actual density of the sintered composite was determined using the Archimedes displacement method, and the theoretical density calculated from Equation (1) was employed to assess the relative density. The results were consistent with the process optimization data presented in Section 2.1. Microstructural analysis was performed using a Zeiss SIGMA 300 field emission scanning electron microscope, employing back-scattered electron imaging (BSE) mode to quantitatively evaluate the uniformity of TiC particle distribution. The results demonstrated that TiC particles were uniformly dispersed within the Fe-2Ni matrix, with an average particle spacing of 8.6 μm and an agglomerate particle proportion below 5%. XRD analysis revealed that the primary diffraction peaks corresponded to α-Fe, TiC, and trace amounts of Fe_3C phases, with no significant TiO_2 or MoO_3 peaks detected, confirming the chemical stability of the reinforcing phase under the specified conditions. Microhardness measurements were taken at 0.1 mm intervals along the cross-section, yielding values ranging from HV 610 to HV 635 with a standard deviation of $\pm$12 HV. Compared to the 96.54% relative density reported by Dong Hulin et al. [7] for the 40% TiC/Fe system, this system achieved a relative density of 98.6% at lower sintering temperatures (1150 °C) and pressures (30 MPa), highlighting the densification advantage attributable to the excellent metallurgical compatibility between the fine TiC powder and the Fe-2Ni matrix. Hardness measurements were taken at intervals of 0.1 mm along the cross-section, with fluctuations ranging from HV 610 to HV 635 and a standard deviation of $\pm$12 HV. The uniformity meets the service requirements of the gear material, demonstrating that the hot-press sintering process exhibits excellent process control over microstructural homogeneity.

C. EXPERIMENTAL DETERMINATION OF BENDING STRENGTH AND CONTACT FATIGUE PERFORMANCE

The bending strength experiment was conducted in accordance with the GB/T 6569–2006 standard, employing a three-point bending loading method with a span of 20 mm and a loading rate of 0.5 mm/min. The average bending strength of the optimal composite material was 1120 MPa, representing an improvement of approximately 36.6% compared to the Fe-2Ni matrix (820 MPa), quantitatively validating the reinforcement effect of TiC on the matrix's load-bearing capacity. Analysis of the fracture morphology revealed that the fracture mode was predominantly transgranular, with TiC particles being cut off rather than experiencing interfacial delamination. This fracture pattern differs from the shear fracture observed by Dong Hulin et al. in the 40% TiC/Fe system (shear angle approximately 45°, fracture strain 6.1%): the latter exhibited higher TiC content and weaker matrix support for the reinforcement phase [8], resulting in a brittle-plastic hybrid fracture behavior; whereas the current system, with a lower TiC content (10 wt%) and superior interfacial bonding quality, demonstrated dominant transgranular fracture and a more stable bending fracture mode, consistent with the conclusion that the interfacial bonding strength exceeds the strength of the TiC particles themselves.

III. EXPERIMENTAL DESIGN FOR FRICTION AND WEAR TESTS AND DETERMINATION OF CHARACTERISTIC PARAMETERS

A. CONFIGURATION OF THE FRICTION AND WEAR TESTING APPARATUS AND SETTINGS FOR OPERATING CONDITIONS

The friction and wear experiments were conducted on the UMT-3 multifunctional friction and wear testing machine [9], employing a pin-on-disc contact configuration. The upper specimen was a composite material pin with a diameter of 6 mm, while the lower specimen was a GCr15 steel disc (hardness HRC 62). The operating parameters were determined based on the gear pitch circle linear velocity range (0.5–3.0 m/s) and contact load range (50–250 N). The experimental protocol specified load gradients of 50 N, 100 N, 150 N, and 200 N, sliding speed gradients of 0.5 m/s, 1.0 m/s, 1.5 m/s, and 2.0 m/s, with a uniform total sliding distance of 1000 μm. The normal force was collected in real-time by a high-precision force sensor (accuracy $\pm$0.1 N), and the friction force signal was continuously recorded at a frequency of 1 Hz by the data acquisition system. Wear measurement was performed using a balance with a precision of 1/10,000 (accuracy 0.1 mg); each experiment was repeated three times, and the average value was taken to control measurement error [10]. The friction coefficient was calculated according to Equation (3):

$$\mu = \frac{F_f}{F_N}, \tag{3}$$

where F_f is friction force and F_N is normal load.

B. THE QUANTITATIVE RELATIONSHIP BETWEEN LOAD AND SLIDING SPEED ON THE FRICTION COEFFICIENT

Under dry friction conditions, the quantitative effects of load and sliding speed on the friction coefficient of the TiC (10 wt%)/MoS_2 (3 wt%)/Fe-2Ni composite material were investigated. As the load increased from 50 N to 150 N, the friction coefficient gradually decreased from 0.132 to 0.082, consistent with the mechanism described by Bowden-Tabor, where an increased actual contact area leads to a relative reduction in interfacial shear stress. When the load further increased to 200 N, the friction coefficient slightly rose to 0.091, attributable to greater abrasive embedding depth under high loads, which elevated the contribution of plowing effects to the friction force. An increase in sliding speed from 0.5 m/s to 1.5 m/s elevated the friction interface temperature, promoting the spreading and densification of the MoS_2 transfer film and resulting in a continuous decrease in the friction coefficient. When the sliding speed exceeded 2.0 m/s, the stability of the lubricating transfer film declined, leading to minor fluctuations in the friction coefficient, indicating a critical stable speed for the MoS_2 transfer film [11]. The distribution data of the friction coefficient under the coupled effects of load and speed are presented in Table 3.

TABLE 3. Steady-State Friction Coefficient Under Different Loads and Sliding Speed Conditions

Load/Speed	0.5 m/s	1.0 m/s	1.5 m/s	2.0 m/s
50 N	0.132	0.121	0.108	0.112
100 N	0.109	0.097	0.088	0.093
150 N	0.088	0.082	0.078	0.084
200 N	0.096	0.089	0.085	0.091

C. THE MECHANISM OF LUBRICATION CONDITIONS ON WEAR RATE AND MATERIAL REMOVAL BEHAVIOR

Lubrication conditions are a key external variable influencing the wear rate of composite materials. The experiment compared the wear rates under three operating conditions: dry friction, boundary lubrication (oil film thickness approximately 0.5 μm), and full-film lubrication (oil film thickness approximately 2.0 μm). Under standard conditions of a load of 150 N and a speed of 1.0 m/s, the dry friction wear rate was 1.8×10^{-5} mm^3/(N·m); under boundary lubrication, it decreased to 5.6×10^{-6} mm^3/(N·m); and under full-film lubrication, it further dropped to 1.2×10^{-6} mm^3/(N·m), representing a reduction of approximately 93%. Regarding material removal behavior, dry friction primarily involved abrasive cutting and plowing, generating substantial sheet-like abrasive debris; under boundary lubrication, the synergistic effect of the lubricating oil film and the MoS_2 transfer film significantly reduced plowing depth, transforming the abrasive debris into fine granular particles; under full-film lubrication, the friction pair was almost completely separated by the oil film, and material removal was dominated by fatigue spalling. Regarding dry friction wear behavior, Dong Hulin et al. also found in pin-disc two-body abrasive wear experiments that as the load increased from 0.5 kg to 2.5 kg, the volumetric wear of the 40% TiC/Fe composite increased from 0.0025 cm^3 to 0.0054 cm^3, with relative wear resistance reaching a peak of 2.67 at a load of 1.5 kg. This pattern aligns physically with the phenomenon of the wear rate growth rate slowing down near a 150 N load in this system: under moderate loads, the hard TiC reinforcement phase maintains full contact with the abrasive and resists wear; excessive loads cause the reinforcement phase to lose matrix support and detach entirely, leading to a renewed increase in the wear rate. Both systems demonstrate that the TiC reinforcement phase exhibits a load-sensitive wear-resistant window, and the service load of the composite material must be controlled within this range to achieve optimal friction reduction [12]. The wear volume (m^3) is expressed according to Archard's wear law as given in Equation (4):

$$V = K \cdot \frac{F_N \cdot L}{H}, \tag{4}$$

where K is the dimensionless wear coefficient, L is the sliding distance (m), H is the material hardness (Pa).

IV. WEAR SURFACE ANALYSIS AND EVALUATION OF COMPOSITE DESIGN EFFICIENCY

A. MICROSCOPIC ANALYSIS OF WEAR SURFACE MORPHOLOGY AND CHIP COMPOSITION

After completing the wear experiment, the wear surfaces of the pin specimens were systematically observed using SEM, while quantitative analysis of chip composition was performed using EDS spectroscopy [13]. Under dry friction conditions with a load of 150 N, the wear surfaces exhibited distinct ploughing grooves features with groove depths ranging from 2.5 to 4.0 μm, accompanied by minor material accumulation at the groove edges, indicating that abrasive wear was the dominant failure mechanism. At a sliding velocity of 1.5 m/s, temperature rise at the friction interface induced surface oxidation; EDS measurements revealed an iron oxide content of approximately 12.4 at% on the wear surfaces, confirming that the oxidative wear mechanism concurrently participated in material removal—a finding consistent with the lubrication analysis conclusions presented in Section 3.3. Chip morphology analysis revealed that under dry friction conditions, chips predominantly exhibited elongated sheet-like shapes with an average length of 65 μm, indicating a dominant cutting removal mode. Under boundary lubrication conditions, chips transformed into nearly spherical fine particles measuring 5–15 μm in diameter, closely correlating with the uniform distribution of shear stress at the friction interface. Quantitative EDS analysis demonstrated that the Ti content in chips (approximately 8.3 at%) was lower than the theoretical TiC content in the composite material, suggesting that TiC particles were preferentially retained within the matrix during wear, providing sustained support for wear resistance. This retention mechanism aligns with the phenomenon observed by Dong Hulin et al. in SEM wear morphology analysis [14]: when the TiC reinforcement content falls within the optimal range, the wear surface exhibits shallow plough grooves and fewer spalling pits, with the reinforcement phase effectively resisting abrasive cutting. Only when the TiC content is excessively high (50 wt%), insufficient matrix support leads to extensive reinforcement spalling, resulting in deep, wide plough grooves and dense spalling pits on the wear surface—a mechanism that closely matches the observed intensified interfacial delamination under the 15 wt% TiC condition in this system.

B. DETERMINATION OF THE DOMINANT WEAR MECHANISM AND THE TRANSFORMATION PATTERNS INDUCED BY OPERATING CONDITIONS

The determination of wear mechanisms is based comprehensively on the surface morphology characteristics of the worn surface, the morphology of wear particles, and the wear rate-load relationship curve. Under low loads ($\leq$ 100 N) and low speeds ($\leq$ 1.0 m/s), the worn surface primarily exhibits parallel furrows without a distinct oxide layer, indicating mild abrasive wear. When the load increases to 150 N or the speed rises to 1.5 m/s, the thickness of the surface oxide layer increases, the friction coefficient stabilizes, and the rate of wear increase significantly slows down, with the mechanism shifting to oxidation-dominated wear—a pattern consistent with the lowest friction coefficient observed in this range as described in Section 3.2. Under high-load (200 N) and high-speed (2.0 m/s) combined conditions, extensive sheet-like pitting defects with depths of 8–12 μm appear on the worn surface, indicating a composite wear mode involving both adhesive wear and delamination wear. The fundamental shift in wear mechanisms results from the synergistic interaction between frictional interface temperature rise and contact stress, as noted by Dong Hulin et al. [15]. The relationship between material hardness H, plow groove depth h_c, and normal load F_N is given by:

$$V = K \cdot \frac{F_N \cdot L}{H}, \tag{4}$$

where φ is the shear angle between the abrasive and the sample surface. This relationship indicates that, with the normal load constant, F_N is inversely proportional to H—the higher the material hardness, the shallower the ploughing grooves and the better the wear resistance. This finding fully aligns with experimental observations that the TiC-reinforced phase effectively enhances surface hardness (HV 620) under high-speed, heavy-load conditions, thereby suppressing ploughing grooves deepening. Furthermore, when the contact stress exceeds the critical ratio of the material's yield stress, additional effects occur ($\sigma_{contact}/\sigma_{yield} > 0.6$). The thickness of the sub surface plastic deformation layer exceeds the critical value, leading to delamination failure, as shown in Figure 2.

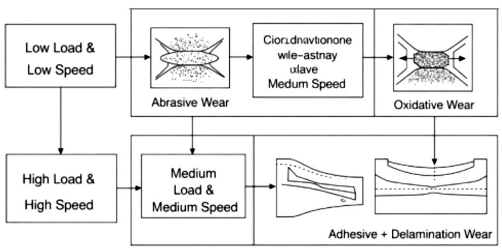

FIGURE 2. Schematic diagram of composition and interfacial bonding structure of TiC/MoS_2/Fe-2Ni composite

C. COMPREHENSIVE EVALUATION OF WEAR RESISTANCE PERFORMANCE AND COMPOSITION OPTIMIZATION DIRECTIONS FOR COMPOSITE MATERIALS

The product of the specific wear rate and friction coefficient serves as the comprehensive evaluation metric for wear resistance. Under standard operating conditions of 150 N and 1.0 m/s, the TiC (10 wt%)/MoS_2 (3 wt%)/Fe-2Ni composite exhibited a comprehensive wear index of 4.6×10^{-7} mm^3/(N·m), representing a reduction of approximately 62% compared to the pure Fe-2Ni matrix (1.2×10^{-6} mm^3/(N·m)). Compared with similar TiC-based single-component reinforced iron composites reported in the literature (wear index approximately 7.0×10^{-7} mm^3/(N·m)), the synergistic incorporation of the MoS_2 lubricating component further enhanced friction-reduction efficiency by about 34%, demonstrating the superiority of dual-component synergistic design over single-reinforcement systems. For future composition optimization, two key approaches should be prioritized: first, modifying the surface of TiC particles through Ti(C,N) coating to establish a core-shell structure, thereby enhancing interfacial bonding strength and reducing reinforcement phase detachment probability; second, exploring hybrid solid lubrication systems that partially replace MoS_2 with WS_2 to improve the thermal stability of the lubricating film under high-temperature conditions ($>$ 400°C), thereby extending the service performance range of the composite to higher speeds and temperatures, meeting the engineering requirements of next-generation high-performance transmissions.

V. CONCLUSION

TiC/MoS_2 composite reinforced Fe-2Ni iron-based powder metallurgy composites were prepared and systematically studied. The optimal sintering process is 1150 °C, 30 MPa, 60 min, with a relative density of 98.6% and microhardness HV 620. The composite with 10 wt% TiC and 3 wt% MoS_2 shows the best synergistic effect, with friction coefficient of 0.08–0.10 and wear rate reduced by 62%. Under load-speed coupling, the wear mechanism transforms from abrasive wear to oxidative wear and slight delamination wear. The stable MoS_2 transfer film is the key to friction reduction. This composite is suitable for high-speed and heavy-load transmission gears and can provide experimental support for the design and engineering application of gear composites.

ACKNOWLEDGMENT

The preferred spelling of the word "acknowledgment" in American English is without an "e" after the "g." Use the singular heading even if you have many acknowledgments. Avoid expressions such as "One of us (S.B.A.) would like to thank ... ." Instead, write "F. A. Author thanks ... ." In most cases, sponsor and financial support acknowledgments are placed in the unnumbered footnote on the first page, not here.

REFERENCES

[1] H. S. Budapanahalli, C. S. Dhaduti, R. Kumar, et al., "A review on aluminium metal matrix composite for tribological study on gear applications," *Discover Applied Sciences*, vol. 8, no. 1, pp. 16–16, 2025, doi: 10.1007/S42452-025-07989-W.

[2] H. Matija and K. Simon, "A fundamental approach to determine the impact of aramid and carbon fibers on durability and tribological performance of different polymer composites demonstrated in gear transmission process," *Journal of Polymer Engineering*, vol. 43, no. 6, pp. 487–496, 2023, doi: 10.1515/POLYENG-2023-0027.

[3] A. V. Alliyankal, J. Nidhin, P. Vishnu, et al., "Tribological and thermogravimetric performance of flax/bamboo hybrid composites for gear applications: Influence of the stacking sequence," *Polymer Composites*, vol. 44, no. 2, pp. 1038–1053, 2022, doi: 10.1002/PC.27152.

[4] A. Durjava, B. Mojškerc, Z. Bergant, et al., "Image-based monitoring of material emissions for wear characterization of laminated polymer composite gears," *Wear*, vol. 590, pp. 206563–206563, 2026, doi: 10.1016/J.WEAR.2026.206563.

[5] M. Jakoby, M. Engels, T. Fahrbach, et al., "A New Electrified Planetary Gear Set—The Cost- and Fuel-Efficient Alternative to Continuously Variable Transmissions," *SAE International Journal of Advances and Current Practices in Mobility*, vol. 8, no. 1, pp. 152–160, 2025, doi: 10.4271/2025-01-0309.

[6] M. Hriberšek and S. Kulovec, "Evaluation of load-carrying and wear resistance of carbon-reinforced composite gears for E-mobility: Short-term versus long-term performance," *Polymer Composites*, vol. 46, no. S3, pp. S63–S82, 2025, doi: 10.1002/PC.29951.

[7] X. Pang, Y. He, X. Chen, et al., "Research on Debris Characteristics and Wear Mechanism of Gear Material 18CrNiMo7-6 Used in Mining Reducer Under Dust-Contaminated Lubrication," *Lubricants*, vol. 13, no. 3, pp. 107–107, 2025, doi: 10.3390/LUBRICANTS13030107.

[8] M. Hriberšek, S. Kulovec, and L. Toubal, "Performance Evaluation of Biocomposite Gears Under Fatigue and Wear: Steel Drive Gear Versus Biocomposite Drive Gear and Biocomposite Drive Gear Versus Biocomposite Gear," *Fatigue & Fracture of Engineering Materials & Structures*, vol. 48, no. 4, pp. 1768–1781, 2025, doi: 10.1111/FFE.14590.

[9] G. R. Ripeanu, M. Tănase, I. A. Portoacă, et al., "Assessing the Tribological Impact of 3D Printed Carbon-Reinforced ABS Composite Cylindrical Gears," *Lubricants*, vol. 12, no. 11, pp. 376–376, 2024, doi: 10.3390/LUBRICANTS12110376.

[10] J. Guan, D. Wu, L. Zhang, et al., "The friction behavior and wear mechanism of RV reducer gear steel (20CrMo) subjected to three different heat treatment processes from -20 °C to 100 °C," *Journal of Materials Research and Technology*, vol. 32, pp. 2609–2623, 2024, doi: 10.1016/J.JMRT.2024.08.120.

[11] I. A. B., M. N. N., and I. A., "Interrelation of wear rates of accelerator gear teeth," *IOP Conference Series: Earth and Environmental Science*, vol. 1284, no. 1, 2023, doi: 10.1088/1755-1315/1284/1/012024.

[12] J. S. Kumar, K. Kaushik, and J. Sudeepan, "Recent advances in tribological properties of silicon based nanofillers incorporated polymer nanocomposites," *Materials Today: Proceedings*, vol. 92, no. P2, pp. 1231–1239, 2023, doi: 10.1016/J.MATPR.2023.05.328.

[13] K. S. S., K. K., C. H. C. N., et al., "Wear, friction behaviour and thermal characteristics of tungsten carbide reinforced polyamide composites for gear applications," *Materials Today: Proceedings*, vol. 37, no. P2, 2020, doi: 10.1016/j.matpr.2020.09.204.

[14] A. Kumar, A. Patnaik, and I. Bhat, "Parametric analysis of tribological for gear materials behaviour and mechanical study of cobalt metal powder filled Al-7075 alloy composites," *Materials Today: Proceedings*, vol. 27, no. Pt 3, pp. 2787–2800, 2020, doi: 10.1016/j.matpr.2019.12.200.

[15] A. Nethula, S. S. N. Koka, R. Chanamala, et al., "Investigations on Thermal, Wear Behavior and Condition Monitoring of Polylactic Acid (PLA)/Thermoplastic Polyurethane (TPU) Composite Gears Enhanced with Silica-Coated TiO_2 (S-TiO_2) Nanoparticles," *Journal of The Institution of Engineers (India): Series D*, vol. 106, no. 2, pp. 1–14, 2024, doi: 10.1007/S40033-024-00712-W.